J Neurophysiol 94: 3836–3848, 2005.
First published August 24, 2005; doi:10.1152/jn.00653.2005.

Dendritic Na^+ Current Inactivation Can Increase Cell Excitability By Delaying a Somatic Depolarizing Afterpotential

Fernando R. Fernandez, W. Hamish Mehaffey, and Ray W. Turner
Hotchkiss Brain Institute, University of Calgary, Calgary, Alberta, Canada

Submitted 23 June 2005; accepted in final form 22 August 2005

Fernandez, Fernando R., W. Hamish Mehaffey, and Ray W. Turner. Dendritic Na^+ current inactivation can increase cell excitability by delaying a somatic depolarizing afterpotential. *J Neurophysiol* 94: 3836–3848, 2005. First published August 24, 2005; doi:10.1152/jn.00653.2005. Many central neurons support active dendritic spike backpropagation mediated by voltage-gated currents. Active spikes in dendrites have been shown capable of providing feedback to the soma to influence somatic excitability and firing dynamics through a depolarizing afterpotential (DAP). In pyramidal cells of the electrosensory lobe of weakly electric fish, Na^+ spikes in dendrites undergo a frequency-dependent broadening that enhances the DAP to increase somatic firing frequency. We use a combination of dynamical analysis and electrophysiological recordings to demonstrate that spike broadening in dendrites is primarily caused by a cumulative inactivation of dendritic Na^+ current. We further show that a reduction in dendritic Na^+ current increases excitability by decreasing the interspike interval and promoting burst firing. This process arises when inactivation of dendritic Na^+ current shifts the latency of the dendritic spike to delay the arrival of the DAP sufficiently to increase its impact on somatic membrane potential despite a reduction in dendritic excitability. Furthermore, the relationship between dendritic Na^+ current density and somatic excitability is nonmonotonic, as intermediate levels of dendritic Na^+ current exert the greatest excitatory influence. These results reveal that temporal shifts in dendritic spike firing provide a novel means for backpropagating spikes to influence the final output of a cell.

INTRODUCTION

In many central neurons examined, the presence of excitatory inward currents in dendrites supports active backpropagation (Spruston et al. 1995; Stuart and Hausser 1994; Stuart et al. 1997; Tank et al. 1988; Turner et al. 1991). Backpropagating events can in turn feed back to the soma and influence excitability by increasing firing frequency or changing overall somatic firing dynamics (Golding et al. 1999; Larkum et al. 1999; Lemon and Turner 2000; Magee and Carruth 1999; Mainen and Sejnowski 1996; Schwindt and Crill 1999). The ability of dendrites to influence somatic activity depends in part on the complement of ion channels that control the shape and dynamics of active dendritic events. It is generally assumed that a loss of inward current in dendrites reduces the overall excitability of a system by reducing the extent that the dendrite can excite the soma.

A detailed account of how backpropagating spikes generate a depolarizing afterpotential (DAP) is found in pyramidal cells of the electrosensory lateral line lobe (ELL) of weakly electric fish (*Apteronotus leptorhynchus*). These neurons receive primary afferent input and generate spike firing that is used for both estimating the peripheral stimulus and detecting specific sensory features (Chacron et al. 2003; Gabbiani et al. 1996; Oswald et al. 2004). We have shown that spikes initiate in the soma/axon hillock region and backpropagate over at least the proximal 200 μm of the apical dendritic tree. A progressive increase in dendritic spike duration during backpropagation generates a DAP at the soma through passive dendro-somatic current flow (Turner et al. 1994). This process occurs with each spike generated in the cell and does not require high-frequency firing or coincident synaptic activation to produce a measurable somatic response. At spike frequencies beyond ~75 Hz, the DAP increases in amplitude and enhances somatic excitability by shortening the interspike interval (ISI) and converting the somatic spike pattern into bursts terminated by high-frequency doublets. The frequency-dependent increase in the DAP arises through dynamic changes in dendritic spikes that include a decrease in spike amplitude and rate of repolarization. The resulting increase in dendritic refractory period works synergistically with the decreasing somatic ISI to produce a conditional spike backpropagation that underlies burst firing (Lemon and Turner 2000; Noonan et al. 2003). Burst firing produced through this mechanism has also been shown to play a critical role in coding low frequency stimulus waveforms both in vitro and in vivo (Chacron et al. 2003; Oswald et al. 2004). In fact, the burst doublet carries specific information concerning amplitude modulations of the afferent stimulus. Hence, understanding the dynamics and biophysics of bursting in ELL pyramidal cells has the potential to reveal novel roles of dendritic excitability on somatic firing dynamics within a well understood sensory processing context.

In this study, we were interested in the dynamics and biophysics that lead to increased firing frequency and burst firing in ELL pyramidal cells. In particular, we wanted to understand the biophysics of dendritic spike broadening, which is critical to the emergence of burst firing and high-frequency doublets. Our previous work has shown the potential for a cumulative K^+ current inactivation in dendrites to underlie the necessary spike broadening. We now show that frequency-dependent dendritic spike broadening relies critically on a cumulative inactivation of dendritic Na^+ currents. Using a dynamical analysis of a reduced model, we show that somatic excitability can be increased with decreased excitability in dendrites through a reduction in steady-state Na^+ current. We corroborate our theoretical findings with experiments that reduce Na^+ current density in the dendrites and increase burst

Address for reprint requests and other correspondence: R. W Turner, Hotchkiss Brain Institute, University of Calgary, 3330 Hospital Dr. N.W., Calgary, Alberta T2N 4N1, Canada (E-mail: rwturner@ucalgary.ca).

The costs of publication of this article were defrayed in part by the payment of page charges. The article must therefore be hereby marked "*advertisement*" in accordance with 18 U.S.C. Section 1734 solely to indicate this fact.

firing frequency. Finally, we show that this occurs when dendritic Na^+ current inactivation increases the delay in arrival of the DAP despite reducing the dendritic depolarization underlying the DAP. This mechanism could be of general relevance to central neurons possessing active dendrites as dendritic Na^+ channels are typically expressed in lower density and thus predispose dendritic Na^+ current to inactivate during high-frequency somatic firing.

METHODS

Animals

Weakly electric fish (*A. leptorhynchus*) were obtained from a local supplier and kept in 26°C water. All experimental protocols were approved by the University of Calgary Animal Resource Center in accordance with the guidelines established by the Canadian Council on Animal Care.

Tissue preparation

All chemicals were obtained from SIGMA (St. Louis, MO) unless otherwise noted. In all cases, recordings were obtained from separate pyramidal cell somata or apical dendrites in in vitro slices. Animals were anesthetized in 0.05% phenoxy-ethanol, and ELL tissue slices of 300–400 μm thickness were prepared as previously described (Turner et al. 1994). Slices were maintained by constant perfusion of artificial cerebrospinal fluid (ACSF; 1–2 ml/min), and superfusion of humidified 95% O_2-5% CO_2 gas. ACSF contained (in mM) 124 NaCl, 3 KCl, 24 $NaHCO_3$, 1.6 $CaCl_2$, 1.2 $MgSO_4$,10 D-glucose, and 0.75 KH_2PO_4, pH 7.4.

Electrophysiology and drug application

Current-clamp microelectrode recordings from the dendrite or soma were obtained using an Axoclamp 2-A amplifier (Axon Instruments) at a sampling rate of 10–40 kHz. Glass microelectrodes were backfilled with 2 M KAc (pH 7.4; 90–120 MΩ resistance). Recordings were made from pyramidal cells in the largest ELL segment receiving P-unit inputs (centromedial segment). Bursting pyramidal cells were identified by their progression from a tonic to a characteristic burst firing mode after sufficient depolarization (Lemon and Turner 2000; Turner et al. 1994). Square wave stimulation pulses were delivered through isolation units (0.1 ms, 1–50 V; Digitimer SIU) to bipolar electrodes (twisted 62-μm nichrome wire) placed on pyramidal cell axons within the plexiform layer. On-cell dendritic voltage-clamp recordings were obtained using a Multiclamp 700A (Axon Instruments) at a sampling rate of 5 kHz. Dendrites were identified by their location in the ELL molecular layer. The patch electrode solution consisted of (in mM) 140 KCl, 5 EGTA, 10 HEPES, and 2.5 $MgCl_2$. The membrane potential in these recordings was estimated from the reversal of the single-channel *I-V* relation. The reversal value was -69.3 ± 2.8 mV ($n = 4$). On-cell patches were stepped from 60 to -50 mV, which translated into a step depolarization from -129 to -19 mV when the cell membrane potential offset was taken into account. All recordings were done at 20–23°C.

TTX was focally applied to dendritic regions by adding it to the electrolyte of an extracellular electrode consisting of (in mM) 148 NaCl, 3.25 KCl, 1.5 $CaCl_2$, 1.5 $MgCl_2$, 10 HEPES, and 20 D-glucose, pH 7.4. Air pressure pulses were used to eject TTX (16 μM) in the dendritic region. A visual estimate of the radius of drug application was initially obtained in dendritic regions of the cerebellar molecular layer under transillumination. Previous studies have shown delays of $\leq$2 min before TTX ejected dorsal to the stratum fibrosum (StF) showed somatic effects (Turner et al. 1994).

Voltage- and current-clamp analysis

Voltage-clamp analysis consisted of fitting the time course of K^+ current inactivation with a single-exponential decay function. Analysis of current-clamp data used custom software written in MatLab 6.5 (MathWorks). Spike threshold was determined through analysis of the voltage derivative. The rate of spike rise was taken as the slope between spike threshold and peak spike height. Area was calculated by integrating membrane voltage from threshold to spike reset. Spike frequency was taken as the average of the inverse of the ISI of the entire spike train. Averaged data are presented as means $\pm$ SE. All tests of statistical significance used paired *t*-test, with significance defined as $P < 0.05$. Data fits were obtained using Origin 7.0, MatLab 6.5, or Clampfit 8.1(Axon Instruments) using a least-squares method.

Simulations

Simulations were constructed in MatLab 6.5 using a fourth-order Runge-Kutta algorithm with a time step (dt) of 0.005 ms. Simulations were also run in XPPAUT 5.91 (Ermentrout 2002) for phase-plane analysis. All bifurcation analyses were done using the XPP-AUTO (Doedel 1981; Ermentrout 2002) package. Our model consisted of a reduction of two compartments (soma and dendrite). This is similar to the approach taken by other authors when reducing bursting mechanisms involving two or more compartments (Doiron et al. 2002; Mainen and Sejnowski 1996; Pinsky and Rinzel 1994; Wang 1999). Our model was described by the following equations

$$m_\infty = \frac{1}{1 + e^{(-(V+40)/3)}} \quad (1)$$

Na^+ activation

$$\frac{dh_s}{dt} = \frac{-h_s + h_{s\infty}(V)}{\tau_{hs}(V)} \quad (2)$$

Na^+ inactivation

$$h_{s\infty} = \frac{1}{1 + e^{((V+40)/3)}} \quad (3)$$

Na^+ steady-state inactivation and K^+ activation

$$\frac{dm_d}{dt} = \frac{-m_d + m_{d\infty}(V)}{\tau_{m_d}(V)} \quad (4)$$

dendritic Na^+ activation

$$m_{d\infty} = \frac{1}{1 + e^{(-(V+46.7)/5.7)}} \quad (5)$$

dendritic steady-state Na^+ activation

$$\frac{dh_d}{dt} = \frac{-h_d + h_{d\infty}(V)}{\tau_{h_d}(V)} \quad (6)$$

dendritic Na^+ inactivation

$$h_{d\infty} = \frac{1}{1 + e^{((V+55)/3)}} \quad (7)$$

dendritic steady-state Na^+ inactivation

$$\frac{dn_d}{dt} = \frac{-n_d + n_{d\infty}(V)}{\tau_{n_d}(V)} \quad (8)$$

dendritic K^+ activation

$$n_{d\infty} = \frac{1}{1 + e^{(-(V+12.5)/8.75)}} \quad (9)$$

dendritic steady-state K^+ activation

All time constants in the model were voltage-dependent and described by a Lorentzian function as used in a previous study (Fernandez et al. 2005)

$$\tau(V) = y_0 + \frac{2Aw}{4\pi(V - V_c)^2 + w^2} \quad (10)$$

for h_s: $V_c = -64$, $w = 28$, $A = 232$, $y_0 = 0$, for m_d: $V_c = -45.7$, $w = 26$, $A = 7.4$, $y_0 = 0$, for h_d: $V_c = -60$, $w = 43$, $A = 301.6$, $y_0 = 0$, and for n_d: $V_c = -40$, $w = 30$, $A = 70$, $y_0 = 0.4$.

Voltage in the somatic and dendritic compartments was integrated according to

$$C_s \frac{dV_s}{dt} = \frac{(V_d - V_s)}{\kappa R} + I_E - g_{Nas} m_\infty^3 h_s (V_s - E_{Na^+}) - g_{Ks}(1 - h_s)^4 (V_s - E_{K^+}) - g_{leaks}(V_s - E_{leak}) \quad (11)$$

$$C_d \frac{dV_d}{dt} = \frac{(V_s - V_d)}{(1 - \kappa)R} - g_{Nad} m_d^3 h_d (V_d - E_{Na^+}) - g_{Kd} n_d^4 (V_d - E_{K^+}) - g_{leakd}(V_d - E_{leak}) \quad (12)$$

Constants in the somatic and dendrite compartments consisted of the following: $C_s = 1.2$ μF/cm^2, $C_d = 3.5$ μF/cm^2, $R = 2/3$, $\kappa = 0.35$, $E_{Na^+} = 40$ mV, $E_{K^+} = -88.5$ mV, $E_{leak} = -72$ mV, $g_{Nas} = 60$ μS/cm^2, $g_{Ks} = 10$ μS/cm^2, $g_{leaks} = 0.18$ μS/cm^2, $g_{Nad} = 20$ μS/cm^2, $g_{Kd} = 8$ μS/cm^2, $g_{leakd} = 0.18$ μS/cm^2.

The parameter κ denotes the relative current influence of the compartments on each other. A κ value of 0.35 signifies that the dendritic current influence on the soma is greater than the somatic current influence on the dendrite. The capacitance in the dendrite was made larger than the somatic value to simulate the difference in total capacitance between the soma and dendrite. The R parameter denotes the resistance between the two compartments. The κ and R values are similar to those of previous modeling studies using this approach (Doiron et al. 2002; Mainen and Sejnowski 1996; Pinsky and Rinzel 1994; Wang 1999).

RESULTS

Dendritic spikes produce a somatic DAP that increases somatic excitability

Backpropagating spikes in ELL pyramidal cells increase somatic excitability, as defined by a decrease in ISI that leads to burst firing. The key element in this process is the frequency-dependent change in dendritic spike properties, reflected as an increase in spike duration and decrease in spike amplitude. The present study focused on the role of the DAP in modifying cell excitability and on the biophysical basis for the frequency-dependent change in dendritic properties that modify the DAP. Both factors can be analyzed effectively at spike frequencies that lead to burst firing.

Ejections of TTX in dendritic regions of pyramidal cells has been used in previous studies to establish that currents underlying the DAP arise from dendritic Na^+ currents (Lemon and Turner 2000; Turner et al. 1994). We repeated this procedure to fully quantify the extent to which a progressive decrease in ISI values during a burst can be attributed to dendritic Na^+ currents. Local dendritic drug ejections are readily applied in the ELL, where diffusion of TTX to the somatic region is hampered by a thick axon tract that separates the pyramidal cell layer and the molecular layer where dendrites project. To ensure that TTX did not block somatic Na^+ channels, we monitored somatic spike height. Under control conditions with sufficient stimulation (0.25–0.7 nA), the somatic ISI decreased with each successive spike in a burst (Fig. 1*A*). The ISI ranged from 7.8 to 5.5 ms for the first two spikes and 4.4 to 3.1 ms for the last two spikes in a burst train. Focal pressure application of TTX at the dendritic level completely eliminated the progressive decrease in somatic ISI (Fig. 1*A*) with ISI values ranging from 9.5 to 6.4 ms but that remained nearly constant throughout the spike train. These experiments establish that dendritic Na^+ currents are critical to a progressive decrease in ISI and thus act as the primary source of an increase in somatic excitability.

Ionic basis for dendritic spike broadening

A critical feature for the decrease in ISI and progression to burst firing is the presence of a dynamic dendritic spike waveform during repetitive firing (Noonan et al. 2003). One proposed explanation for a broadening of the dendritic spike is a cumulative inactivation of dendritic K^+ current. Frequency-dependent spike broadening through cumulative inactivation of K^+ currents has been shown in numerous systems (Aldrich et al. 1979; Ma and Koester 1995, 1996; Shao et al. 1999). In our system, this process could ensure an increase in the amount of current flow to the soma after each somatic spike. In this regard, ELL pyramidal cell dendrites express Kv3.3 K^+ channels (Rashid et al. 2001a,b) that have been reported to exhibit a slow rate of inactivation (Rudy et al. 1999). In a previous modeling study, we considered the potential for these channels to undergo a cumulative inactivation sufficient to support dendritic spike broadening (Doiron et al. 2001, 2002). We found that the slow rates of inactivation recorded for Kv3.3 channels in HEK cells and in outside-out recordings of K^+ channels in pyramidal cell proximal apical dendrites were insufficient to promote this process. However, this study did establish the potential for a fast inactivating dendritic K^+ current to broaden dendritic spikes, and in so doing, trigger the entire process of conditional backpropagation. Since that time we established that Kv3.3 channels in heterologous expression systems can show a very rapid rate of inactivation depending on translation (Fernandez et al. 2003). Others have shown that the rate of inactivation of K^+ currents can be markedly affected by cytosolic proteins, giving rise to the possibility for regional control of dendritic K^+ channel inactivation (Nadal et al. 2003). We thus reexamined the potential for K^+ currents recorded in mid-dendritic regions to exhibit an inactivation fast enough to promote dendritic spike broadening. To test this we used on-cell patch-clamp recordings 150–200 μm from the soma to measure the rate of K^+ current inactivation. Our voltage-clamp protocol consisted of depolarizing the dendritic patch to -19 mV from -129 mV holding potential (assuming a membrane rest potential of -69 mV, see METHODS) using a step protocol. On-cell dendritic recordings revealed 3–6 channels per patch (Fig. 1*B*). Ensemble averages revealed that the time constant of inactivation was 1,086 $\pm$ 87 ms (Fig. 1*B*; $n = 6$). This is significant in that this slow rate of inactivation is orders of magnitude outside the time scale of a single ISI in pyramidal cells and is therefore unlikely to contribute to the process that underlies spike broadening during a burst. This does not conflict with the important effects of dendritic K^+ channels in modifying baseline spike properties that control burst threshold (Noonan et al. 2003), but it does implicate other

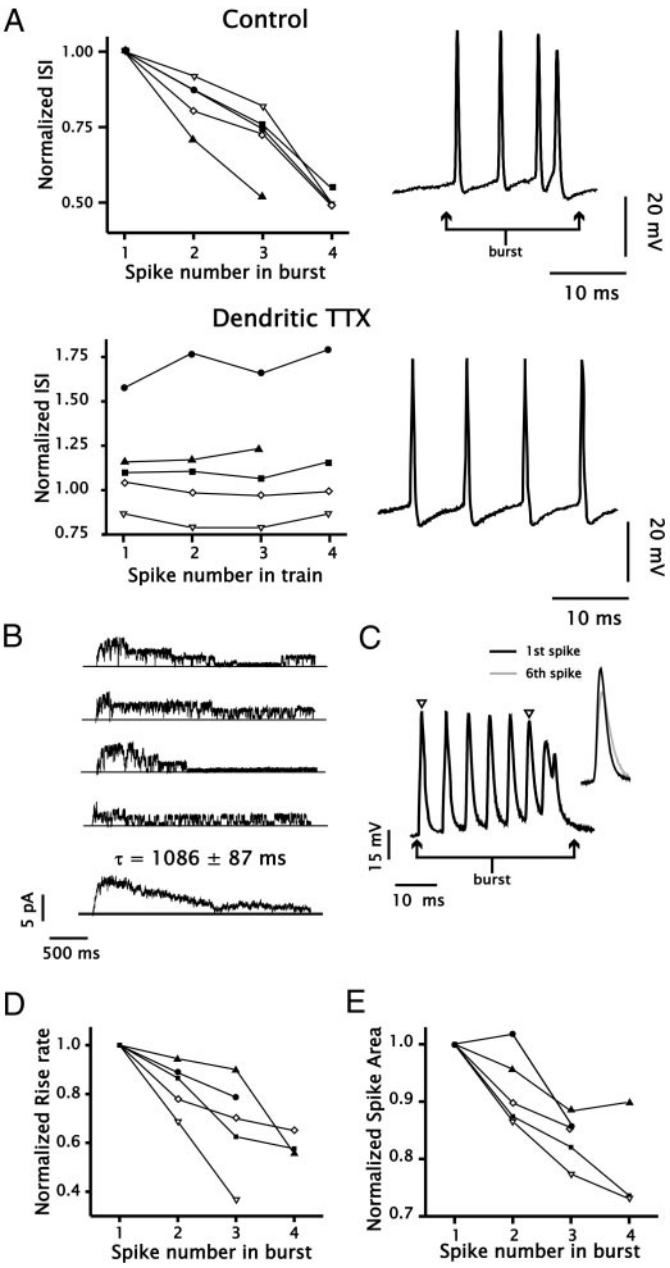

FIG. 1. Changes in dendritic spike properties underlie an increase in somatic excitability. *A*: plots of somatic interspike interval (ISI) during a single burst for 5 separate cells recorded in control condition and after focal application of TTX in the dendritic region. All ISIs are normalized to the 1st ISI in the control recording. Each cell is represented by a different symbol. *Right*: representative case of somatic spike firing in the control and TTX condition. *B*: cell-attached patch recordings of K^+ channels from electrosensory lateral line lobe (ELL) pyramidal cell dendrites (150–200 μm from cell body). Membrane potential was stepped from −129 to −19 mV for 4 s using a step depolarization. Ensemble averages were constructed by averaging 6–8 sweeps. Inactivation was fit with a single exponential decay function. *C*: representative voltage trace from a dendritic recording during burst firing. The cell was depolarized until burst firing threshold was reached. *Inset*: the 1st (*black*) and 6th (*gray*) dendritic spikes superimposed for comparison. *D* and *E*, plots of dendritic spike rate of rise (*D*) and area (*E*) during burst firing for 5 separate cells. Each cell is represented by a different symbol. The last dendritic spike was not included due to contamination from the 2nd spike of the terminating doublet. Dendritic spike rate of rise and area are normalized to the 1st spike in the burst.

ion channels as the driving force behind dendritic spike broadening.

Spike broadening can also be brought on through cumulative Na^+ current inactivation (Fleidervish et al. 1996; Van Goor et al. 2000). Indeed, dendritic Na^+ currents in hippocampal CA1 cells have been found to be particularly susceptible to cumulative inactivation (Colbert et al. 1997; Jung et al. 1997). Sodium current inactivation reduces the rate of rise and repolarization of the spike that reduces spike height and in turn the activation of repolarizing K^+ current. These properties in fact resemble the progression of change in ELL pyramidal cell dendritic spikes during a burst, making cumulative Na^+ current inactivation a good candidate mechanism for spike broadening. We found that direct patch-clamp recordings of Na^+ current were not feasible in pyramidal cells due to a relatively low conductance of single Na^+ channels compared with K^+ currents, and a density of Na^+ current below that required to provide even single-channel recordings in the on-cell configuration. This result is likely due to an established punctate distribution of Na^+ channels in apical dendrites (Turner et al. 1994), and is consistent with the very small diameter (~2 μm) and high-input resistance (>250 MΩ) of pyramidal cell dendrites requiring very few Na^+ channels to sustain spike conduction. We thus used spike rate of rise, which has been previously established as a good indicator of Na^+ inactivation (Azouz and Gray 2000), as well as the total area underneath a dendritic spike to assess Na^+ current inactivation in dendrites. We used dendritic microelectrode recordings (100–150 μm from the pyramidal cell layer) to drive burst firing and record dendritic spikes (Fig. 1*C*). In all cells, the rate of dendritic spike rise (Fig. 1*D*) and the area underneath the spike (Fig. 1*E*) decreased as spike firing within a burst progressed. This decrease could be substantial in attaining up to a 60% decline in spike rate of rise within the first four spikes of a burst. These results implicate Na^+ current inactivation as a possible source for spike broadening, DAP growth, and the transition to bursting. These data also reveal the surprising result that an overall reduction in dendritic Na^+ current (a decrease in dendritic excitability) accompanies the increase in cell excitability during a burst. Note, however, that a complete absence of Na^+ currents in dendrites decreases excitability as shown in Fig. 1*A* and indicates that the relationship between dendritic Na^+ current density and somatic excitability is not monotonic.

Role of dendritic Na^+ current inactivation as revealed in a reduced model

To gain a better understanding of how cumulative dendritic Na^+ inactivation can affect cell excitability, we built a reduced phenomenological model. The reduced model consisted of a single dendritic compartment coupled to a soma. The two compartments influenced each other through a current term that was proportional to the difference in voltage between the two compartments and scaled by terms representing the resistance between the compartments and the size of the compartments. This approach has been used previously in our system and in numerous models of mammalian bursting neurons (Doiron et al. 2002; Mainen and Sejnowski 1996; Pinsky and Rinzel 1994; Rinzel and Ermentrout 1998; Wang 1999). The reduction allows a dynamical analysis that can test the possible role of Na^+ current inactivation in burst firing dynamics in a simple

biophysical system. Note that this form of analysis is not possible with large-scale compartmental models due to the number of variables. Our model contained two currents in each compartment. The somatic currents included a fast Na^+ current and a K^+ current. To reduce the dimensionality of the model, we assumed that inactivation of somatic Na^+ current was directly proportional to the K^+ current and that the Na^+ activation variable equilibrated with voltage instantaneously (see METHODS). The dendrite contained a Na^+ current with slightly slower activation and inactivation kinetics relative to the soma. The K^+ current in the dendrite was independent of Na^+ current inactivation with a more positive steady-state voltage relationship than in the somatic compartment. We found that spike broadening in dendrites required slightly slower kinetics of Na^+ current and a lower density in the dendrites, consistent with numerous studies on dendritic Na^+ currents (Colbert et al. 1997; Jung et al. 1997; Stuart and Hausser 1994; Turner et al. 1994).

ELL pyramidal cell bursting is characterized by a transition from tonic to burst firing with increased current injection (Lemon and Turner 2000; Turner et al. 1994). Like the cell, the model reproduced this phenomenon as well as the shape of the DAP during bursting in terms of a progressive increase in DAP amplitude through a spike train (Fig. 2, *A* and *B*). The model also reproduced the drop in dendritic spike area during bursting to a similar extent as that measured in the pyramidal cell (Fig. 2*C*), a key result which was not captured by previous models of bursting (Doiron et al. 2002). The dendritic spike rate of rise and the extent of Na^+ current available in the dendrite also decreased during the build-up phase of the burst (Fig. 2*D*). These results are important in showing that an overall drop in dendritic excitability is associated with an increase in somatic excitability through a decrease in ISI that leads to burst firing.

The coupling between the two compartments was critical for the burst pattern to emerge. If the resistance between the two compartments was decreased ($R < 0.9$), the voltage trajectory of the dendritic spike closely followed that of the somatic compartment and no bursting pattern emerged. Thus under these conditions, no significant transient difference in voltage was formed between the two compartments and thus no DAP could be generated. With increased resistance ($R > 1.5$), the ability of the dendritic spike to influence the soma was reduced, such that transient differences in voltage between the two compartments generated very little current at the soma and reduced the amplitude of the DAP. With further increases in R the ability of the dendrite to generate a spike and induce burst firing at the soma was eliminated.

In addition to a decrease in Na^+ current availability in the dendrites, the model revealed a drop in peak K^+ current with each spike in a burst, a result attributable to the decrease in spike height (Fig. 3*A*). We hypothesized that a drop in K^+ current may amplify the effects of Na^+ current inactivation on dendritic spike width and thus the development of the burst. To test this, we used the model to reset the n_d variable controlling dendritic K^+ current immediately before each dendritic spike peak. The n_d variable was reset to 0.78, the value maintained at tonic firing frequencies that do not induce a shift to burst firing. We found that the reset maintained dendritic K^+ current at the peak of the dendritic spike constant without affecting the overall dynamics of the current at other stages in the firing process (Fig. 3*B*). Although the reset of the n_d variable increased burst threshold, it did not prevent bursting. This is consistent with previous experiments that established an important role for dendritic K^+ currents in setting burst threshold in pyramidal cells (Noonan et al. 2003). These results suggest

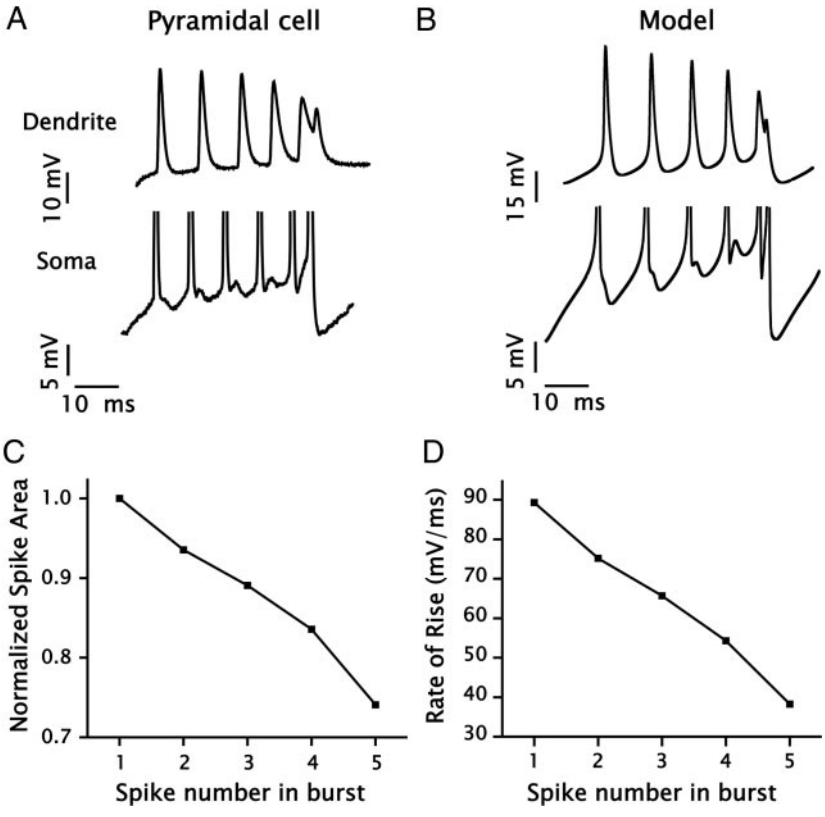

FIG. 2. Model of the ELL pyramidal cell that incorporates dendritic Na^+ inactivation produces burst firing. *A* and *B*: representative pyramidal cell recordings at the level of dendrites (*top*) and soma (*bottom*) compared with that obtained in a reduced model (*B*). Dendritic and somatic recordings are from different cells and somatic spikes are clipped to improve visualization of the depolarizing afterpotential (DAP). Note that the model generates the entire process leading to a burst, including an increase in DAP amplitude during repetitive firing and a terminating spike doublet, as well as evidence for a temporal shift in the peak of the DAP (*A* and *B*, *bottom*). *C*: plot of dendritic spike area during burst firing in the model cell illustrates a progressive decrease in area with each spike in a burst. *D*: plot of dendritic spike rate of rise during burst firing in the model cell illustrates a progressive decrease in rate of rise with each spike in a burst.

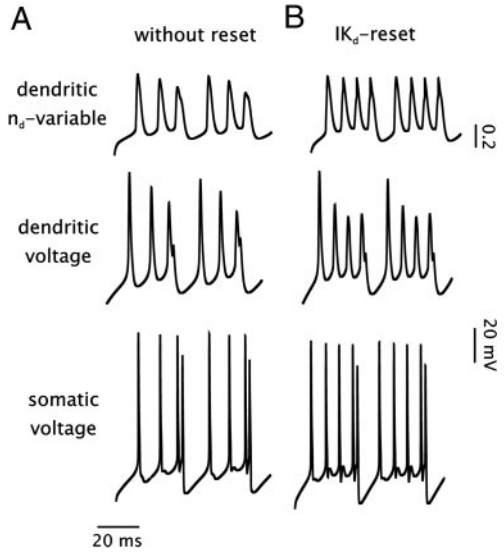

FIG. 3. Decrease in dendritic K^+ current is not required for burst firing in the model. *A* and *B*: comparison of the model with and without an imposed reset of the dendritic K^+ current. *A*: model in burst firing mode ($I_E = 15\ \mu A/cm^2$) with normal dendritic K^+ current (*without reset*). During burst firing, the variable controlling dendritic K^+ current (n_d) decreases due to the inactivation of dendritic Na^+ current and subsequent drop in spike height. *B*: model in burst firing mode ($I_E = 22\ \mu A/cm^2$) with a reset to maintain peak dendritic K^+ current constant in the face of a decrease in spike amplitude. The n_d variable is reset at the moment that the derivative of dendritic voltage crosses 0.05 mV/ms in a negative-going direction and dendritic voltage is greater than −20 mV. This corresponds to a point ~0.25 ms before peak dendritic spike voltage. Note that in the presence of a K^+ current reset burst firing still occurs but with slightly altered dynamics, indicating that dendritic K^+ current regulates rather than underlies burst firing.

that K^+ current in the dendrites plays a secondary but important role in amplifying the burst process. This does not rule out the potential for a modulation of dendritic K^+ current to change burst threshold or its contribution during a burst. However, our model suggests that cumulative inactivation of Na^+ current in dendrites is the primary factor driving dendritic spike broadening and is both necessary and sufficient to induce burst firing.

To summarize, under normal conditions, the cumulative inactivation of Na^+ current reduces the rate of rise of the dendritic spike, which broadens the spike and reduces its amplitude. The reduction in spike height in turn decreases the activation of K^+ current and results in a further broadening by reducing the rate of spike repolarization. The decrease in K^+ current activation also results in a slightly more positive interspike voltage of dendritic spikes (peak change about ~4 mV), which increases the amount of excitatory current from the dendrite to the soma by making the dendritic voltage more positive than the soma. Together the reduction in the spike rate of rise and repolarization significantly broadens the dendritic spike. Thus dendritic Na^+ current inactivation alters spike properties during a burst through combined effects on both Na^+- and K^+-dependent components of spike firing.

Analysis of pyramidal cell model and experimental confirmation

The preceding results show that a decrease in Na^+ current in the dendrite leads to an increase in excitability and the onset of burst firing. To identify the dynamics governing the burst process in our system, we performed a dynamical analysis on the model. This approach allows us to analyze a large range of model behaviors and understand the dynamics that mediate transitions in the model.

To first obtain a qualitative measure of model behavior, we measured the frequency-current (*F-I*) relation in the model and compared it to data obtained from ELL pyramidal cells. ELL pyramidal cells typically have a *F-I* relation that starts at very low mean firing frequency (~6 Hz) that is linear through a large frequency range but begins to saturate at the upper frequency range (>175 Hz; Fig. 4*A*). At firing frequencies between 80 and 150 Hz, pyramidal cells will typically start bursting, with a range in burst frequency from 20 to 80 Hz (Fig. 4*A*). In the control case in the model, the *F-I* relation was within the range of values measured in pyramidal cells. At around 5 $\mu A/cm^2$ of current injection at the soma, the model started firing at frequencies <5 Hz and maintained a tonic firing range to ~80 Hz (Fig. 4*B*). At ~12.3 $\mu A/cm^2$ of current, the model started bursting. Under different densities of dendritic Na^+ current (gNa_d), the model behaved qualitatively similar to the control case, with a clear tonic range that began firing <5 Hz and a bursting region that could be distinguished by a sudden change in the slope of the *F-I* relation (Fig. 4*B*). Lowering dendritic gNa_d, however, lowered the frequency at which bursting emerged and increased the gain of the *F-I* relation. This was most noticeable in the model when the lowest gNa_d value (15 $\mu S/cm^2$) was compared with the case with the highest gNa_d value (25 $\mu S/cm^2$; Fig. 4*B*). When these curves are compared, it is clear that the model with the lowest gNa_d value had a larger gain that resulted in burst firing occurring at a lower current input. Because bursting involves the generation of a doublet, we also considered the effect of not counting the doublet on the *F-I* relation and whether lowering gNa_d still increased the gain of the *F-I* relation. Under these conditions, the *F-I* relation continued to have a larger gain for the case with the lowest gNa_d value (15$\mu S/cm^2$; Fig. 4*C*). Note, however, that threshold firing slightly increased with lower gNa_d values in the dendrites. Thus although gain was increased and burst threshold was reduced the onset of tonic firing required slightly higher levels of current (~0.5 $\mu A/cm^2$).

The effects of changing gNa_d on the model was most clearly visualized when all frequencies were measured and plotted rather than averaged as in the preceding text. Thus for every current step, individual ISI times were converted into a frequency measure and plotted. In the tonic range, there was no variability in firing frequency, and thus every point was superimposed (Fig. 4, *D–F*). In the bursting regime, however, ISI times were variable, and the emergence of bursting could be clearly visualized in the *F-I* relation as a scatter in the frequency values measured (Fig. 4, *D–F*). As shown in the preceding text, lowering gNa_d decreased burst threshold and caused the scattering of frequency values (indicative of bursting) to emerge at a lower firing frequency (Fig. 4*D*) compared with control (Fig. 4*E*). Furthermore, when gNa_d was increased, the scatter of frequency values emerged at a higher firing frequency and current input (Fig. 4*F*). Note that the scatter in the firing frequency during bursting is indicative of chaotic bursting and consistent with a previous study on ELL pyramidal cell bursting dynamics (Doiron et al. 2002). Thus under certain current input values, the system displayed the most variability in firing frequency, as indicated by the almost continuous representation of frequency values from 50 to 500

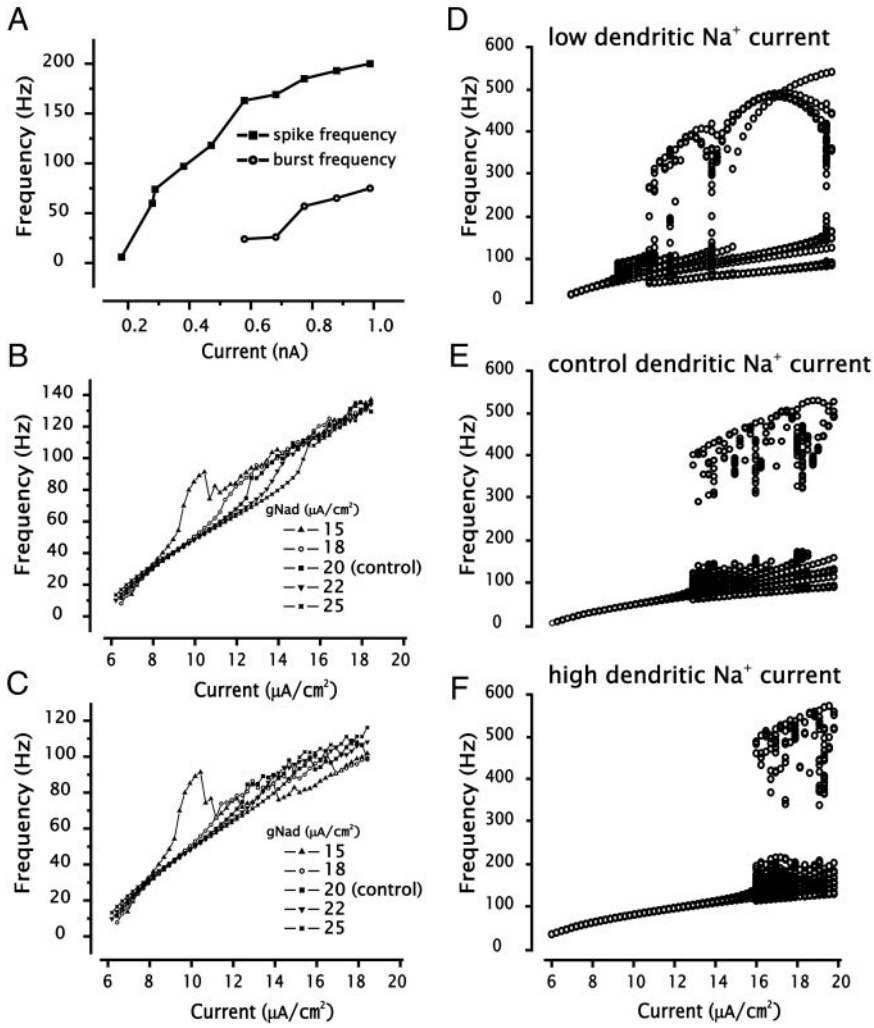

FIG. 4. Frequency-current plots in the model under different dendritic Na^+ current densities. *A*: representative frequency-current plot for an ELL pyramidal cell. The cell was held at −82 mV using −0.275 nA of current injection and step depolarized by adding a current step ranging from 0.15 to 1.0 nA. Frequency was calculated as the mean firing frequency during the 175-ms current step. At ~0.5 nA, the cell starting bursting with a burst frequency of 22 Hz. *B* and *C*: frequency-current relations for the model during tonic firing and burst firing calculated as the mean frequency with (*B*) and without (*C*) the burst doublet using different densities of dendritic Na^+ current (gNa_d) during a 300-ms step depolarization ranging from 6 to 19 $\mu A/cm^2$. *D–F*: frequency-current relations for the model with low (*D*, 18 $\mu A/cm^2$), control (*E*, 20 $\mu A/cm^2$), and high (*F*, 22 $\mu A/cm^2$) levels of gNa_d. Frequency-current relations were constructed by plotting all frequency values without averaging. The model was run for 5 s, and all frequencies binned into their corresponding current values. Note that at burst threshold (I_E = 8.7–16.0 $\mu A/cm^2$), firing frequency values become scattered. Also note that burst threshold and the generation of high-frequency spikes occurred at lower current inputs with lower dendritic Na^+ current.

Hz. The *F-I* relationships of the model suggested that lower Na^+ current density in the dendrites can increase gain, firing frequency, and lower burst threshold. Note that the complete absence of dendritic Na^+ current reduced excitability as it reduced the gain of the *F-I* relation and removed the increase in ISI values (no burst firing), which was similar to the application of TTX in the cell.

Neuronal bursting can generally be divided into slow and fast subsystems (Rinzel and Ermentrout 1998). Specifically, the dynamics of spike generation can be considered as a fast subsystem, whereas the underlying burst dynamics are caused by a second subsystem operating on a significantly slower time scale. This separation can be used to allow the analysis of bursting separately from the dynamics of spike generation. In our model, the critical slow variable driving a decrease in ISI times and bursting is the cumulative inactivation of dendritic Na^+ current. This variable has a voltage-dependent time constant that ranges from 4.5 to 0.5 ms from peak negative to peak positive voltage, respectively. This range of time constants is consistent with numerous studies on voltage-dependent Na^+ currents (Hille 2001). Because of the range in time constants, dendritic Na^+ current inactivation participates in both the fast and slow subsystems in our bursting model. By having slow time constants at more negative voltages (e.g., between spikes), the recovery of the variable is slow enough to permit accumulation of Na^+ current inactivation. The variable is fast enough, however, at more positive voltages (e.g., during the spike) to participate in spike generation and to shape spike waveform through inactivation. Thus our system lacks an explicit slow variable, the participation of which is limited to the slow subsystem, which makes carrying out an analysis of bursting dynamics in two times scales difficult. During a burst in the dendrites, the decrease in the h_d variable slowly accumulates until a doublet is generated in the soma. The doublet is then followed by a burst AHP in the soma and a transient quiescent period in the dendrite that provides sufficient time for recovery of the h_d variable before the start of the next burst (Fig. 5, *A* and *B*). This process can be clearly visualized if the solution trajectories of the h_d and V_d variables are plotted against each other (Fig. 5*B*). The general decrease in the magnitude of h_d is associated with smaller amplitude oscillations that eventually terminate in a doublet and the recovery of the h_d variable.

To understand the dynamics governing the transitions from quiescence to tonic firing and tonic firing to burst firing, we carried out a bifurcation analysis of our model. In brief, a bifurcation analysis consists of tracking fixed points (e.g., a steady-state) or limit cycles (e.g., action potential) while changing a parameter in the model. Changing a model parameter can lead to fixed-points or limit cycles being created or destroyed, which is associated with basic dynamical changes in

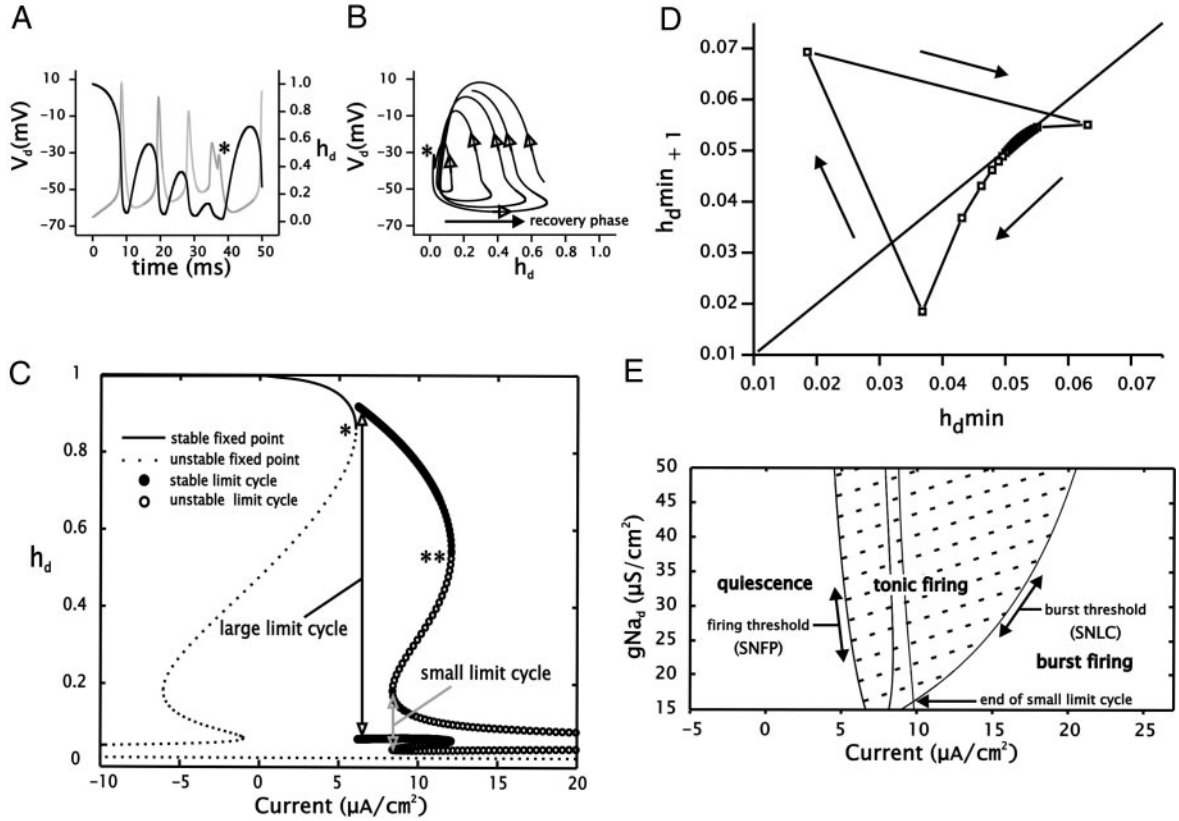

FIG. 5. Analysis of model dynamics reveals opposite effects of dendritic Na^+ current density on tonic and burst firing threshold. *A*: plot of dendritic voltage (V_d, gray line) and the variable controlling dendritic Na^+ inactivation (h_d, black line). *B*: solution trajectories for bursting in the phase plane of V_d and h_d. Hollow arrowheads indicate direction of flow. Note that as dendritic spike height drops the h_d variable decreases. This occurs until the dendrite fails to produce a spike in response to the doublet in the soma (*), at which point the dendritic voltage decreases for a sufficient amount of time to recover the h_d variable (filled arrow). *C*: bifurcation analysis of model using somatic current injection (I_E) as the bifurcation parameter. The h_d variable is plotted with I_E as it most clearly shows all fixed points and limit cycles. During the quiescent phase ($I_E < 6.05$ $\mu A/cm^2$), 3 fixed points exist (stable: solid line, 2 unstable: dashed lines). At $I_E = 6.05$ $\mu A/cm^2$, the stable and unstable saddle fixed points coalesce (*) in a saddle node bifurcation of fixed points (SNFP), forming a stable limit cycle (filled circles) and correspond to the tonic firing threshold. At $I_E = 12.15$ $\mu A/cm^2$ the stable (filled circles) and unstable limit cycles (unfilled circles) coalesce (**) in a saddle node bifurcation of limit cycles (SNLC), corresponding to burst threshold. *D*: $h_d$min return map for a single burst cycle in the model. The model was run for 550 ms with $I_E = 12.9$ $\mu A/cm^2$. The $h_d$min was calculated as the lowest value of the h_d varible within a single spike cycle. Arrows indicate the direction of the sequence. *E*: 2 parameter bifurcation of model using dendritic Na^+ current density (gNa_d) and I_E as the bifurcation parameters. The SNFP and SNLC points (*C*) were tracked as a function of gNa_d and I_E to gauge the effects of dendritic Na^+ current on tonic and burst firing thresholds.

a system. We chose somatic current injection as the bifurcation parameter as it can induce transitions experimentally. As shown in Fig. 5*C*, the model has three fixed points at rest (0 $\mu A/cm^2$): two unstable (dashed lines) and one stable (solid line). With increased current injection, the stable point and the unstable saddle point coalesce in a saddle node bifurcation of fixed points (*). At this point, a stable limit cycle (filled circles) is formed that produces the tonic firing range in the model. Because the limit cycle is formed through a saddle node of fixed points, spike generation arises at arbitrarily low firing frequencies (Rinzel and Ermentrout 1998; Strogatz 1994). All firing models in which the approach to threshold is through a saddle node bifurcation have been termed type I (Ermentrout 1996). This is in contrast to type II neurons in which the limit cycle is formed through a Hopf bifurcation and firing begins at some minimal frequency (Ermentrout 1996). Our model being type I is consistent with experimental results in our system because pyramidal cells have a very large frequency range and firing begins at low frequencies. Note also the presence of a second but smaller stable limit cycle. This indicated that our model had bi-rhythmicity due to the co-existence of two stable limit cycles. In numerical simulations, however, this limit cycle was accessible using only a small range of initial conditions and did not mediate any of the dynamic transitions in the control model, making it intractable to test its presence experimentally. With increased current injection the system increases firing frequency until the large stable and unstable limit cycles coalesce in a saddle node of limit cycles (Fig. 5*C*, **). At this point, the system lacks a stable periodic solution and chaotic bursting ensues, consistent with an increase in variability of ISI at burst threshold. The model predicts that burst firing, like tonic firing, begins at arbitrarily low frequencies (defined as the time between consecutive doublets) due to the saddle node of limit cycles (Rinzel and Ermentrout 1998; Strogatz 1994). Thus at current levels slightly above burst threshold the time between doublets can be very large and becomes arbitrarily large as current levels approach burst threshold. The bursting dynamics of the model can also be summarized in a one-dimensional return map using the local h_d-variable minimum ($h_d$min) following a dendritic spike (Fig. 5*D*). The return map was generated using a single burst cycle with a current input of 12.9 $\mu A/cm^2$, which was slightly above burst threshold. As the burst cycle progresses, the $h_d$min values start decreasing in arbitrarily small increments as shown by the

numerous points collected near the diagonal line. At some time point the rate of decrease of $h_d$min begins to increase and reaches a low point that signifies the doublet. After $h_d$min has reached its lowest point, it recovers to its maximal value, which corresponds to the burst AHP. The process is then repeated with the $h_d$min value once again decreasing. This is consistent with a previous theoretical and experimental study, which termed this form of bursting type I due to its dynamical similarities with type I firing (Laing et al. 2003).

Considering that our data and model have shown that dendritic Na^+ inactivation is critical for a decrease in ISI and burst output, we chose to further analyze this parameter. Using somatic current injection and dendritic Na^+ current density as the parameters of interest in a two parameter bifurcation, we tracked the points associated with the thresholds for tonic and burst firing (Fig. 5*D*). As mentioned in the preceding text, tonic and burst threshold in the model were associated with saddle nodes of fixed points (SNFP) and limit cycles (SNLC), respectively. We also tracked the points associated with the start and end of the small limit cycle. The SNFP point occurred at higher current levels when dendritic Na^+ current density is decreased (Fig. 5*E*). Thus the threshold for tonic firing increased as $g\mathrm{Na}_d$ was decreased. Lowering $g\mathrm{Na}_d$, however, had the opposite effect on burst threshold, as the SNLC point occurred at lower current levels as $g\mathrm{Na}_d$ was decreased. In fact, lowering $g\mathrm{Na}_d$ had a much larger effect on burst threshold than on tonic firing threshold because the SNLC shifted by a larger amount on the current axis in the two-parameter bifurcation diagram than the SNFP. Thus lowering overall Na^+ current in the dendrites lead to an increase in excitability by lowering burst threshold and increasing burst firing frequency. Furthermore, this indicates that during a burst in the control condition ($g\mathrm{Na}_d$ = 20 μS/cm^2), the inactivation of dendritic Na^+ current is responsible for burst firing and the decrease in ISI.

Decreasing $g\mathrm{Na}_d$, however, decreased burst threshold over a limited range of $g\mathrm{Na}_d$ values. Lowering $g\mathrm{Na}_d$ below a critical point ($g\mathrm{Na}_d$ < 4.75 μS/cm^2) eliminated the dendritic spike altogether and bursting was no longer possible. Thus the relationship between dendritic Na^+ current density and excitability is nonmonotonic. Note that transitions to bursting at low levels of $g\mathrm{Na}_d$ were mediated through the end of the small limit cycle. This, however, did not change the qualitative aspects of bursting as it was still characterized by a gradual decrease in ISI.

The preceding analysis shows that decreasing Na^+ current in the pyramidal cell dendrite increased cell excitability and burst frequency at a fixed current input level by reducing burst threshold. Although it is impossible to precisely control this parameter experimentally, we reasoned that diffusion of TTX after focal ejections in the slice preparation could be used to induce a transient partial block of Na^+ current in dendrites that would increase burst frequency. To accomplish this, we recorded from pyramidal cells and focally applied TTX in the dendrites. Diffusion from the site of ejection ensures that the dendrite will transiently experience a continuum of local TTX concentrations, so that testing the possible implication of intermediate levels of Na^+ channel density on bursting dynamics is possible. These tests in fact revealed that the application of TTX in dendrites increased burst frequency transiently from 28.1 ± 3.1 to 56.3 ± 8.1 Hz (P < 0.002; n = 4) before abolishing bursting entirely (Fig. 6*C*). In some cases, dendritic TTX also caused bursting to shift into doublets, similar to the model with intermediate levels of $g\mathrm{Na}_d$. The model and experimental results are thus in agreement and indicate that an

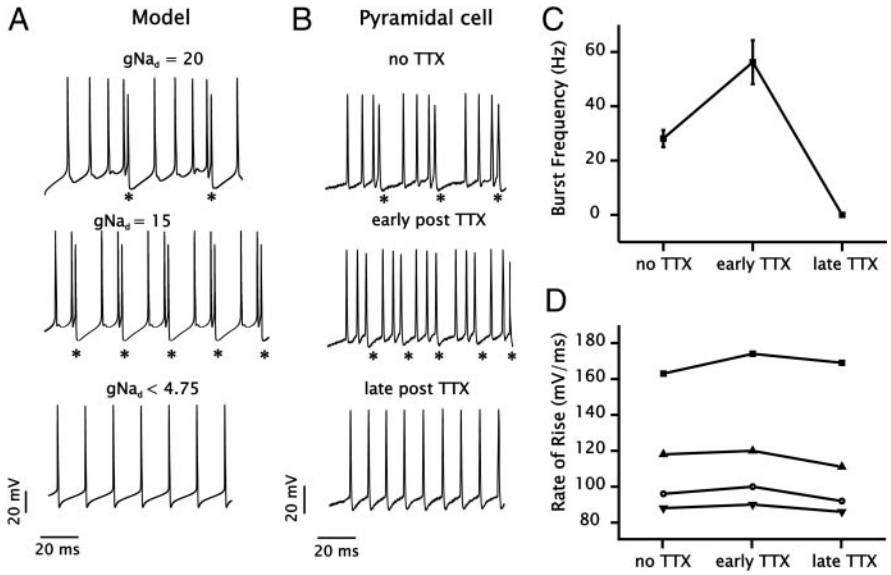

FIG. 6. A reduction in dendritic Na^+ current density increases burst firing frequency in both the model and pyramidal cell. *A*: Model response to I_E = 15.5 μA/cm^2 using values of $g\mathrm{Na}_d$ that correspond to control (20 μS/cm^2, *top*), intermediate (4.75–20 μS/cm^2, *middle*), and low levels (<4.75 μS/cm^2, *bottom*). In the model, burst frequency for any given I_E is highest with intermediate levels of $g\mathrm{Na}_d$. *B*: ELL pyramidal cell response to focal dendritic application of TTX using a constant 0.75 nA of driving current. Intermittent ejections and diffusion in the extracelluar medium permits TTX concentrations to vary through a range of concentrations analogous to the control, intermediate, and low levels of $g\mathrm{Na}_d$ in the model. Immediately after TTX application the drug has no effect. Within 2–6 s (*middle*) TTX begins blocking some dendritic Na^+ channels and after 30 s (*bottom*) channel block is complete and the cell responds only with tonic firing. *Asterisks* denote burst AHP at the end of each burst. *C*: plot of burst frequency in control and TTX conditions. Note that application of TTX transiently increases burst firing frequency compared with control before abolishing bursting altogether. *D*: Plot of the rate of rise for the somatic spike for the cells quantified in *D* during control and TTX conditions. Note that despite the application of TTX in the dendrites the rate of rise of the somatic spike was not affected, indicating that TTX effects were restricted to the dendritic region.

intermediate level of dendritic Na^+ channel inactivation can increase overall system excitability, leading to burst firing. To ensure that the experimental results in Fig. 6*C* were not the result of TTX diffusing into the pyramidal cell layer, we monitored the available somatic Na^+ current by measuring the rate of rise of the somatic spike at each stage of the experiment. As shown in Fig. 6*D*, there was no significant change in the rate of rise for the somatic spikes for all the cells tested, indicating that all effects of TTX on cell excitability were mediated entirely at the dendritic level.

Dendritic Na^+ current inactivation increases excitability by delaying the DAP

We next sought to determine the biophysical mechanism by which a net decrease in dendritic excitability could translate to an increase in somatic excitability and a shift to burst firing. We considered that the primary effect of dendritic Na^+ current inactivation was to broaden the dendritic spike as well as delay the time to peak. We hypothesized that these changes could translate to a shift in the arrival of the peak DAP current at the soma. Combining this with a broader dendritic spike would also extend the amount of time the DAP influenced the soma and thus render both a shift in DAP peak and duration. To test this, we measured the time to peak of the DAP or dendritic spike during repetitive antidromic stimulation. Antidromic stimulation was used as it permits precise control of firing rate and a consistent reference point. All recordings of somatic DAP and dendritic waveforms were performed on different cells as simultaneous dual recordings were not possible in this age of animal. Neither the DAP nor dendritic spike increased in latency if the stimulus frequency was below that known to induce a shift from tonic to burst firing (not shown). However, stimulus frequencies ranging from 140 to 200 Hz induced distinct changes in DAP shape (Fig. 7, *A* and *B*). Specifically, with each successive spike the peak of the DAP increased in amplitude and shifted away from the somatic spike by 120 to 190% (Fig. 7, *A and B*; $n = 5$). We next recorded from dendrites during antidromic stimulation to determine if the time to peak voltage of the dendritic spike also shifted to a later time. Indeed, in all cells (stimulus frequencies >140 Hz) the time to peak of the dendritic spike shifted within a train of spikes, ranging from a 105 to 135% delay (by the 4th spike) compared with the first spike (Fig. 7*C*).

The appearance of a larger DAP at the soma is then likely due to the fact that as the DAP shifts away from the somatic spike it also moves away from the spike AHP and arrives at a time with less repolarizing current. Although bursting dynamics have been previously analyzed using a separation of time scales into slow and fast subsystems, the h_d variable participates within both time scales in the burst. This shared variable prevents a separation of time scales. Rather, to further investigate the dynamics, we considered the phase response curve (PRC) of a neuron. In essence, the PRC is a function that relates the position of a perturbation in the spike cycle with its corresponding influence on the phase of the cycle (advance or delay). A PRC is determined by briefly exciting a system at different points of the oscillation phase (Hansel et al. 1995; Rinzel and Ermentrout 1998; Winfree 1980). At each point of excitation, the corresponding advance or delay of the oscillation is measured. In the past, PRCs have been considered when

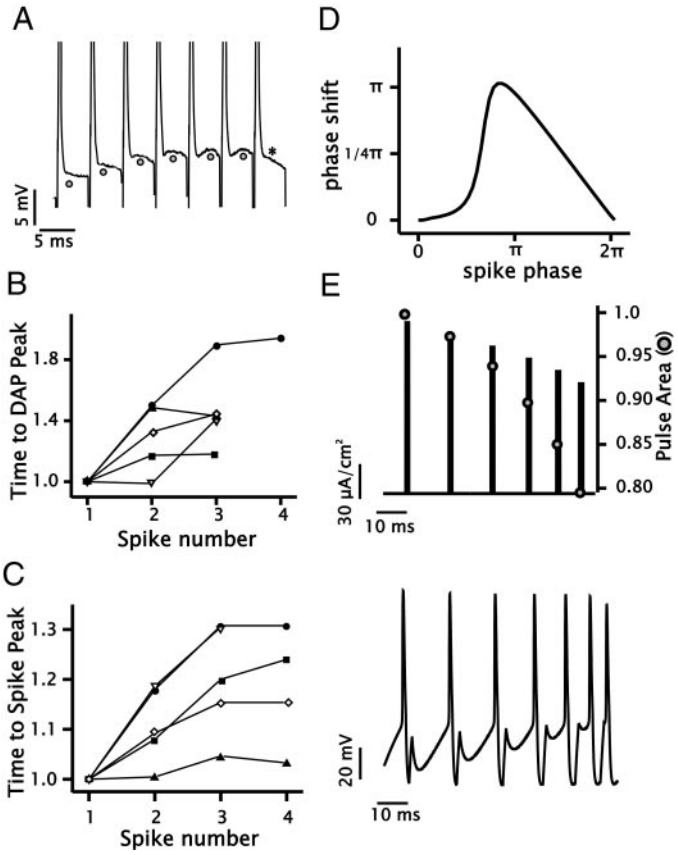

FIG. 7. Dendritic Na^+ current inactivation increases somatic excitability by delaying the DAP. *A*: pyramidal cell somatic recording during antidromic stimulation at 200 Hz. Note that the peak of the DAP (*circle*) shifts away from the somatic spike until abruptly failing (*), signifying the loss of backpropagation. *B*:*C*, Plots of the time to peak of the DAP (*B*) and dendritic spike peak (*C*) during antidromic stimulation for five separate cells (shown by different symbols). Antidromic stimulation frequencies varied from 140 to 200 Hz, and peak latencies are normalized to the first spike in the train. In all cells recorded the DAP and dendritic spike peak latency increases during repetitive simulation. *D*: phase response curve (PRC) for the model without the dendritic compartment. Phase cycle is calculated from the peaks of the spike with 0 to 2π denoting the distance between two consecutive spike peaks. The phase advance is calculated as the reduction in phase cycle length compared with the control (no pulses) that is evoked with pulses ($I_E = 140$ μA/cm^2 for 0.42 ms) delivered at different locations in the phase cycle. *E*: time course of pulses delivered to the model without a dendrite (*top*) and corresponding voltage response (*bottom*). Note that pulses are applied at increasing times after the spike. Each successive pulse is also reduced in height and increased in width to simulate DAP dynamics during bursting, generating a further gradual decrease in area of each successive pulse to 78% of its initial value (*gray filled circle*).

studying synaptic activation of neurons at different points in the spike cycle or in weakly coupled networks of neurons (Hansel et al. 1995; Reyes and Fetz 1993; Rinzel and Ermentrout 1998). Theoretical and computational studies have shown that the qualitative shape of the PRC depends on the dynamics that lead to the formation of a stable limit cycle (Ermentrout 1996; Hansel et al. 1995). For example, type I dynamics in which firing arises through a saddle node bifurcation are associated with PRCs that range from no phase advance to an advance but never a delay (Ermentrout 1996; Hansel et al. 1995). This is in contrast to type II dynamics in which firing arises through a Hopf bifurcation (e.g., Hodgkin-Huxley model) and an excitatory pulse immediately following the

spike delays the next spike, while pulses coming later in the spike cycle can advance the phase (Ermentrout 1996; Hansel et al. 1995).

To analyze the effect of DAP timing in our system, we equated the arrival of the DAP at the soma to a brief excitatory current pulse. Because the transition from quiescence to tonic firing is associated with a saddle node bifurcation of fixed points, the dynamics of our system is type I and the PRC should indicate either zero or positive phase advances. To confirm this we, first removed the dendritic compartment from our model to ensure that there was no additional current source when measuring the PRC. A bifurcation analysis confirmed that type I dynamics were preserved (supplementary Fig. 1)[1]. We next determined the PRC of our model near threshold (I_E = 3.8 μA/cm^2; Fig. 7*D*). The PRC indicated that excitatory pulses arriving immediately after the peak of the spike (phase = 0) have a minimal ability to advance the phase, whereas excitatory pulses arriving some time after the peak of the spike can advance the phase (Fig. 7*D*). As a qualitative test of DAP dynamics on somatic excitability, we excited the model during tonic firing at 65 Hz (I_E = 13.8 μA/cm^2) and added current pulses at different times after the peak of the somatic spike (Fig. 7*E*). We also made each successive excitatory pulse slightly shorter (from 140 to 90 μA/cm^2) and wider (from 0.42 to 0.52 ms), but with an overall decrease in the area (from 1 to 0.78; Fig. 7*E*). This was done to simulate the influence of dynamic changes in the dendritic waveform during a burst and the decrease in dendritic excitability on the DAP. Despite the fact that each pulse in the train decreased progressively in amplitude, the positive shift in location of the pulse in the phase cycle was sufficient to compensate and increase the phase advance and the firing frequency of the system. Note that the last pulse (number 6) generated a doublet and even reproduced the slight drop in somatic spike height associated with doublets during bursting (Fig. 7*F*). Furthermore, the "pulse-DAP" voltage response became larger despite the fact that the underlying current was actually smaller (Fig. 7*F*).

In summary, our data show that dendritic Na^+ current inactivation and a decrease in dendritic excitability can lead to an overall increase in neuronal excitability. This occurs by increasing somatic firing frequency and facilitating a transition to bursting. This can be achieved because the somatic spike generating system benefits more from a delay in the arrival of the DAP than an increase in its magnitude.

DISCUSSION

Excitable currents in dendrites have numerous functions. These include influencing somatic firing dynamics (Lemon and Turner 2000; Mainen and Sejnowski 1996; Pinsky and Rinzel 1994; Turner et al. 1994; Wang 1999), amplifying synaptic signals (Magee and Johnston 1995), and spike-timing-dependent plasticity (Dan and Poo 2004; Magee and Johnston 1997). Within the context of spike firing at the soma it is generally assumed that an increase in dendritic inward currents (Na^+ or Ca^{2+}) increases overall neuronal excitability. Clearly, a complete absence of inward currents in dendrites will reduce excitability. The relationship between dendritic inward current and somatic excitability, however, is not necessarily monotonic. The present study examined the role of dendritic waveforms on somatic dynamics within the context of a bursting mechanism. We have shown that frequency-dependent spike broadening in ELL pyramidal cell dendrites is initiated by dendritic Na^+ current inactivation. Despite a decrease in dendritic excitability, the soma responds by increasing firing frequency and burst firing, representing an increase in overall system excitability.

A particularly novel result was finding that the principal consequence of dendritic Na^+ current inactivation is to shift the peak time of the dendritic spike waveform and increase overall spike duration. These effects translate into a more effective DAP at the soma by producing a corresponding shift in DAP peak and duration, despite a reduction in dendritic peak voltage. The temporal relation between the DAP and somatic spike are thus more important than the magnitude of the dendritic waveform producing the DAP. This is possible because the soma responds preferentially to excitatory pulses coming later in the spike phase cycle as shown by a PRC analysis. This work thus identifies a novel mechanism by which dynamic changes in the properties of backpropagating dendritic spikes can shift the influence of dendritic membrane in determining the final output of a cell.

Role of K^+ current in dendritic spike broadening

Although K^+ current inactivation can play a significant role in spike broadening in some systems (Aldrich et al. 1979; Ma and Koester 1995, 1996; Shao et al. 1999), our recordings of dendritic K^+ current diminish the possible influence of cumulative K^+ current inactivation because the inactivation time constant was well outside the time frame of a single burst. Indeed, in our model, the decrease in dendritic K^+ current during repetitive firing was not an essential feature in the actual production of a burst. We have shown, however, a definite role for dendritic K^+ current in amplifying spike broadening when the decrease in spike height brought on by Na^+ current inactivation decreases K^+ current activation. This result is fully consistent with our earlier work indicating an important role for dendritic K^+ channels in establishing burst threshold (Noonan et al. 2003). Thus we distinguish cumulative Na^+ current inactivation as the primary source of dendritic spike broadening during repetitive burst firing, with K^+ current playing a secondary regulatory role in amplifying the effects of Na^+ current on dendritic waveforms.

Firing dynamics in the soma influence DAP effects

In our model, the dynamics that produced tonic firing occurred through a saddle node bifurcation of fixed points and thus is a type I firing system. A more experimentally tractable characteristic of type I firing systems is that spike firing frequency can be arbitrarily low, which is consistent with ELL pyramidal cells (Rinzel and Ermentrout 1998). Additionally, type I firing dynamics have a nonnegative PRC (Ermentrout 1996; Hansel et al. 1995). Within the context of our mechanism this means that the DAP can advance the phase of the cycle and increase somatic firing frequency. It is important to note, however, that the effects of a temporal shift in the DAP has the

[1] The Supplementary Material for this article (a figure) is available online at http://jn.physiology.org/cgi/content/full/00653.2005/DC1

potential to produce different effects in other cell types. In Type II firing systems, spike firing starts at a defined minimal frequency because the limit cycle is formed through a Hopf bifurcation (Rinzel and Ermentrout 1998). More importantly, the PRC of type II neurons can be negative in the early part of the phase cycle (Ermentrout 1996; Hansel et al. 1995). A DAP, which is locked to the occurrence of a somatic spike, is likely to fall within the negative region of the PRC and delay the onset of the next spike. Thus the ability of dendritic currents underlying a DAP to excite or inhibit a soma could depend critically on the firing dynamics leading up to threshold.

General applicability of mechanism

Cumulative inactivation is common to many Na^+ and Ca^{2+} currents. The dynamics that govern an increase in somatic firing frequency and transition to bursting in ELL pyramidal cells are thus likely to be generally applicable. Previous studies in neocortical and hippocampal pyramidal cells have shown that an active dendritic spike can lead to a DAP (Golding et al. 1999; Larkum et al. 1999; Magee and Carruth 1999; Schwindt and Crill 1999). In most of these cases, the influence of the DAP in terms of burst firing is detected upon the additional influence of coincident synaptic inputs or secondary to the activation or block of other dendritic ion channels. Nevertheless, inactivation of dendritic Na^+ channels and loss of dendritic spike height can be even more prominent in hippocampal and neocortical pyramidal cells at high frequencies of firing (Jung et al. 1997; Williams and Stuart 2000). Fundamentally, if inactivation of dendritic inward currents leads to a longer dendritic waveform with respect to a somatic spike, there is the possibility of increasing somatic firing rate and excitability by shifting the associated DAP. Again, we predict that the dynamics leading to firing threshold (type I vs. type II) will determine if the DAP is excitatory or inhibitory. Cells that exhibit the characteristics that define a type II firing pattern have been identified (Tateno et al. 2004), yet the full range of cells that fall in this category remains to be explored. A shift in the latency of dendritic spikes and the DAP could then have varied effects depending on cell type.

Our mechanism could also be potentially modulated by synaptic inputs. Synaptic activity and membrane depolarization at the dendritic level could reduce the amount of available steady-state Na^+ current. This is in turn would broaden the active dendritic waveform and increase somatic firing rate through a shift in the arrival of the DAP at the soma. This mechanism would take advantage of the nonlinearities associated with the dendritic waveform and DAP effects on the soma to amplify small depolarizations in the dendrite and their final influence on cell output. Nonlinearities arising from the voltage dependence of NMDA receptors have already been shown to help boost distal synaptic inputs (Polsky et al. 2004; Schiller et al. 2000). In our system, the DAP would be continuously influencing somatic firing rate such that synaptic depolarization in dendrites could inactivate Na^+ channels and decrease burst threshold.

While the biophysics of our current burst model are different from previous models, the underlying dynamics mediating the transitions from quiescence to tonic firing and tonic to burst firing are similar. In previous studies assuming K^+ current inactivation as the source of dendritic spike broadening, it was shown that a saddle-node bifurcation of limit cycles mediates the transition to burst firing (Doiron et al. 2002). Our new model, however, is more consistent with experimental results from K^+ and Na^+ currents and shows that Na^+ current inactivation is capable of reproducing virtually all known properties of burst firing in these cells. Therefore our work represents a refinement of the original reduced model that reveals a novel soma-dendritic interaction in spike firing (Doiron et al. 2002). Interestingly, these findings also indicate that disparate biophysical mechanisms can lead to the same fundamental firing and burst dynamics. In fact, a recent study found that very different parameters in a model of the crab stomatogastric network could lead to similar network bursting properties (Prinz et al. 2004).

In conclusion, we show that in ELL pyramidal cells an increase in cell excitability and transition to bursting is paradoxically mediated by a progressive loss of Na^+ current in dendrites. Our model and experimental data further show that the relationship between dendritic Na^+ current and system excitability is not a monotonic relationship as intermediate levels of dendritic Na^+ current produce the lowest threshold for burst firing. These findings thus reveal a new mechanism by which the influence of backpropagating dendritic spikes on cell output can shift according to the firing history of a cell and the instantaneous temporal relationship between somatic and dendritic spike firing.

ACKNOWLEDGMENTS

We gratefully acknowledge the technical assistance of M. Kruskic and comments on the manuscript by L. Maler, B. Doiron, B. E. McKay, and M. L. Molineux.

GRANTS

This work was supported by Canadian Institute of Health Research, CIHR Doctoral Studentships, and Alberta Provincial Graduate Scholarships to F. R. Fernandez and W. H. Mehaffey and an Alberta Heritage Foundation for Medical Research Scientist Award to R. W. Turner.

REFERENCES

Aldrich RW Jr, Getting PA, and Thompson SH. Mechanism of frequency-dependent broadening of molluscan neurone soma spikes. *J Physiol* 291: 531–544, 1979.

Azouz R and Gray CM. Dynamic spike threshold reveals a mechanism for synaptic coincidence detection in cortical neurons in vivo. *Proc Natl Acad Sci USA* 97: 8110–8115, 2000.

Chacron MJ, Doiron B, Maler L, Longtin A, and Bastian J. Non-classical receptive field mediates switch in a sensory neuron's frequency tuning. *Nature* 423: 77–81, 2003.

Colbert CM, Magee JC, Hoffman DA, and Johnston D. Slow recovery from inactivation of Na^+ channels underlies the activity-dependent attenuation of dendritic action potentials in hippocampal CA1 pyramidal neurons. *J Neurosci* 17: 6512–6521, 1997.

Dan Y and Poo MM. Spike timing-dependent plasticity of neural circuits. *Neuron* 44: 23–30, 2004.

Doedel E. A program for the automatic bifurcation analysis of autonomous systems. *Congre Nemer* 30: 265–484, 1981.

Doiron B, Laing C, Longtin A, and Maler L. Ghostbursting: a novel neuronal burst mechanism. *J Comput Neurosci* 12: 5–25, 2002.

Doiron B, Longtin A, Turner RW, and Maler L. Model of gamma frequency burst discharge generated by conditional backpropagation. *J Neurophysiol* 86: 1523–1545, 2001.

Ermentrout B. Type I membranes, phase resetting curves, and synchrony. *Neural Comput* 8: 979–1001, 1996.

Ermentrout B. *Simulating, Analyzing, and Animating Dynamical Systems: A Guide to XPPAUT for Researchers and Students.* Philadelphia, PA: Society for Industrial and Applied Mathematics, 2002.

Fernandez FR, Mehaffey WH, Molineux ML, and Turner RW. High-threshold K^+ current increases gain by offsetting a frequency-dependent increase in low-threshold K^+ current. *J Neurosci* 25: 363–371, 2005.

Fernandez FR, Morales E, Rashid AJ, Dunn RJ, and Turner RW. Inactivation of Kv3.3 potassium channels in heterologous expression systems. *J Biol Chem* 278: 40890–40898, 2003.

Fleidervish IA, Friedman A, and Gutnick MJ. Slow inactivation of Na^+ current and slow cumulative spike adaptation in mouse and guinea pig neocortical neurons in slices. *J Physiol* 493: 83–97, 1996.

Gabbiani F, Metzner W, Wessel R, and Koch C. From stimulus encoding to feature extraction in weakly electric fish. *Nature* 384: 564–567, 1996.

Golding NL, Jung HY, Mickus T, and Spruston N. Dendritic calcium spike initiation and repolarization are controlled by distinct potassium channel subtypes in CA1 pyramidal neurons. *J Neurosci* 19: 8789–8798, 1999.

Hansel D, Mato G, and Meunier C. Synchrony in excitatory neural networks. *Neural Comput* 7: 307–337, 1995.

Hille B. *Ion Channels of excitable Membranes.* Sunderland, MA: Sinauer, 2001.

Jung HY, Mickus T, and Spruston N. Prolonged sodium channel inactivation contributes to dendritic action potential attenuation in hippocampal pyramidal neurons. *J Neurosci* 17: 6639–6646, 1997.

Laing CR, Doiron B, Longtin A, Noonan L, Turner RW, and Maler L. Type I burst excitability. *J Comput Neurosci* 14: 329–342, 2003.

Larkum ME, Zhu JJ, and Sakmann B. A new cellular mechanism for coupling inputs arriving at different cortical layers. *Nature* 398: 338–341, 1999.

Lemon N and Turner RW. Conditional spike backpropagation generates burst discharge in a sensory neuron. *J Neurophysiol* 84: 1519–1530, 2000.

Ma M and Koester J. Consequences and mechanisms of spike broadening of R20 cells in *Aplysia californica. J Neurosci* 15: 6720–6734, 1995.

Ma M and Koester J. The role of K^+ currents in frequency-dependent spike broadening in *Aplysia* R20 neurons: a dynamic-clamp analysis. *J Neurosci* 16: 4089–4101, 1996.

Magee JC and Carruth M. Dendritic voltage-gated ion channels regulate the action potential firing mode of hippocampal CA1 pyramidal neurons. *J Neurophysiol* 82: 1895–1901, 1999.

Magee JC and Johnston D. Synaptic activation of voltage-gated channels in the dendrites of hippocampal pyramidal neurons. *Science* 268: 301–304, 1995.

Magee JC and Johnston D. A synaptically controlled, associative signal for Hebbian plasticity in hippocampal neurons. *Science* 275: 209–213, 1997.

Mainen ZF and Sejnowski TJ. Influence of dendritic structure on firing pattern in model neocortical neurons. *Nature* 382: 363–366, 1996.

Nadal MS, Ozaita A, Amarillo Y, Vega-Saenz de Miera E, Ma Y, Mo W, Goldberg EM, Misumi Y, Ikehara Y, Neubert TA, and Rudy B. The CD26-related dipeptidyl aminopeptidase-like protein DPPX is a critical component of neuronal A-type K^+ channels. *Neuron* 37: 449–461, 2003.

Noonan L, Doiron B, Laing C, Longtin A, and Turner RW. A dynamic dendritic refractory period regulates burst discharge in the electrosensory lobe of weakly electric fish. *J Neurosci* 23: 1524–1534, 2003.

Oswald AM, Chacron MJ, Doiron B, Bastian J, and Maler L. Parallel processing of sensory input by bursts and isolated spikes. *J Neurosci* 24: 4351–4362, 2004.

Pinsky PF and Rinzel J. Intrinsic and network rhythmogenesis in a reduced Traub model for CA3 neurons. *J Comput Neurosci* 1: 39–60, 1994.

Polsky A, Mel BW, and Schiller J. Computational subunits in thin dendrites of pyramidal cells. *Nat Neurosci* 7: 621–627, 2004.

Prinz AA, Bucher D, and Marder E. Similar network activity from disparate circuit parameters. *Nat Neurosci* 7: 1345–1352, 2004.

Rashid AJ, Dunn RJ, and Turner RW. A prominent soma-dendritic distribution of Kv3.3 K^+ channels in electrosensory and cerebellar neurons. *J Comp Neurol* 441: 234–247, 2001a.

Rashid AJ, Morales E, Turner RW, and Dunn RJ. The contribution of dendritic Kv3 K^+ channels to burst discharge in a sensory neuron. *J Neurosci* 21: 125–135, 2001b.

Reyes AD and Fetz EE. Effects of transient depolarizing potentials on the firing rate of cat neocortical neurons. *J Neurophysiol* 69: 1673–1683, 1993.

Rinzel J and Ermentrout B. Analysis of neural excitability and oscillations. In: *Methods in Neuronal Modeling*, edited by Koch C and Segev I. Cambridge, MA: MIT Press, 1998, p. 251–291.

Rudy B, Chow A, Lau D, Amarillo Y, Ozaita A, Saganich M, Moreno H, Nadal MS, Hernandez-Pineda R, Hernandez-Cruz A, Erisir A, Leonard C, and Vega-Saenz de Miera E. Contributions of Kv3 channels to neuronal excitability. *Ann NY Acad Sci* 868: 304–343, 1999.

Schiller J, Major G, Koester HJ, and Schiller Y. NMDA spikes in basal dendrites of cortical pyramidal neurons. *Nature* 404: 285–289, 2000.

Schwindt P and Crill W. Mechanisms underlying burst and regular spiking evoked by dendritic depolarization in layer 5 cortical pyramidal neurons. *J Neurophysiol* 81: 1341–1354, 1999.

Shao LR, Halvorsrud R, Borg-Graham L, and Storm JF. The role of BK-type Ca^{2+}-dependent K^+ channels in spike broadening during repetitive firing in rat hippocampal pyramidal cells. *J Physiol* 52: 135–146, 1999.

Spruston N, Schiller Y, Stuart G, and Sakmann B. Activity-dependent action potential invasion and calcium influx into hippocampal CA1 dendrites. *Science* 268: 297–300, 1995.

Strogatz SH. *Nonlinear Dynamics and Chaos: With Applications to Physics, Biology, Chemistry, and Engineering.* Reading, MA: Addison-Wesley, 1994.

Stuart G and Hausser M. Initiation and spread of sodium action potentials in cerebellar Purkinje cells. *Neuron* 13: 703–712, 1994.

Stuart G, Spruston N, Sakmann B, and Hausser M. Action potential initiation and backpropagation in neurons of the mammalian CNS. *Trends Neurosci* 20: 125–131, 1997.

Tank DW, Sugimori M, Connor JA, and Llinas RR. Spatially resolved calcium dynamics of mammalian Purkinje cells in cerebellar slice. *Science* 242: 773–777, 1988.

Tateno T, Harsch A, and Robinson HP. Threshold firing frequency-current relationships of neurons in rat somatosensory cortex: type 1 and type 2 dynamics. *J Neurophysiol* 92: 2283–2294, 2004.

Turner RW, Maler L, Deerinck T, Levinson SR, and Ellisman MH. TTX-sensitive dendritic sodium channels underlie oscillatory discharge in a vertebrate sensory neuron. *J Neurosci* 14: 6453–6471, 1994.

Turner RW, Meyers DE, Richardson TL, and Barker JL. The site for initiation of action potential discharge over the somatodendritic axis of rat hippocampal CA1 pyramidal neurons. *J Neurosci* 11: 2270–2280, 1991.

Van Goor F, LeBeau AP, Krsmanovic LZ, Sherman A, Catt KJ, and Stojilkovic SS. Amplitude-dependent spike-broadening and enhanced Ca(2+) signaling in GnRH-secreting neurons. *Biophys J* 79: 1310–1323, 2000.

Wang XJ. Fast burst firing and short-term synaptic plasticity: a model of neocortical chattering neurons. *Neuroscience* 89: 347–362, 1999.

Williams SR and Stuart GJ. Backpropagation of physiological spike trains in neocortical pyramidal neurons: implications for temporal coding in dendrites. *J Neurosci* 20: 8238–8246, 2000.

Winfree AT. *The Geometry of Biological Time.* New York: Springer Verlag, 1980.